SIMULATION OF DRAG CRISIS IN FLOW PAST A CIRCULAR CYLINDER USING 2D COMPUTATIONS

S.P. Singh and S. Mittal*

Abstract

The unsteady incompressible 2D Navier-Stokes equations are solved using a finite element method with Streamline-Upwind/Petrov-Galerkin (SUPG) and Pressure-Stabilizing/Petrov-Galerkin (PSPG) stabilization terms for high Reynolds number (10^5 to 10^6) flow past a cylinder to simulate drag-crisis. The mean drag coefficient for various Re are compared with experimental data. It is observed that the flow at $Re = 10^6$ separates much later, from the cylinder surface as compared to that at $Re = 10^5$. The wake at $Re = 10^6$ is narrower than that at $Re = 10^5$. The time-averaged flow field shows a standing bubble just downstream of the flow separation point for the $Re = 10^5$ flow. The bubble is not observed for the flow at $Re = 10^6$. The energy spectrum of the flow exhibits the characteristics of 2D isotropic turbulence.

Introduction

Drag crisis is a sudden drop in the drag experienced by a body as the Reynolds number is increased beyond a certain critical value. For a smooth circular cylinder the critical Reynolds number at which the drag-crisis occurs is 2×10^5, approximately. The event is marked by transition of the boundary layer, from laminar to turbulent. The turbulent boundary layer results in delay of flow separation over the surface of the cylinder. The separation point is located at 82° from the stagnation point for $Re = 2 \times 10^5$ flow. It moves to 120 deg for the $Re = 10^6$ flow [1]. This leads to an increase in the base pressure and a reduction in the drag coefficient. One of the objectives of the present work is to look into the possibility of predicting drag-crisis via 2D simulations. This is expected to increase our understanding of this phenomenon.

Flow past a cylinder [2] becomes three-dimensional at a value of *Re* as low as 140-190. Hence quantities like the mean drag and base pressure are not expected to be predicted correctly using 2D computations. But their variation with respect to the *Re* should be predicted, at least in a qualitative sense, if the drag crisis is indeed a two-dimensional phenomenon. Selvam [3] has presented his results for 2D Large Eddy Simulation (LES) of flow past a circular cylinder. He observes the drag-crisis but not to the same extent as indicated by the measurements. Further, the phenomenon of drag crisis is observed only if the law of Van Driest damping is utilized. Tamura et.al. [4] have carried out computation without any turbulence model with a third order upwind finite difference scheme in two and three dimensions. Their computations have been able to predict drag crisis for certain grids. However, on increasing the number of grid points, the drag coefficient at $Re = 10^6$ increases significantly. In the present work, no turbulence model is being utilized. We have found from our recent studies that the viscosity introduced by the stabilization terms in the finite element formulation dominates the eddy viscosity from an LES model [5]. Similar observations have been made by Mittal and Moin [6] in the context of higher order finite difference schemes.

It is well known that the transition of flow past a cylinder begins beyond $Re = 200$. In this paper we investigate the presence of inertial range in the energy spectrum of the flow. The results are compared with the behaviour of energy spectrum for 2D isotropic turbulence.

Governing Equations

Let $\Omega \subseteq R^{n_{sd}}$ and $(0, T)$ be the spatial and temporal domains respectively, where n_{sd} is the number of space dimensions, and let Γ denote the boundary Ω. The spatial and temporal co-ordinates are denoted by x and t. The

* Associate Professor, Department of Aerospace Engineering, Indian Institute of Technology Kanpur, Kanpur-208 016, India
E-mail: smittal@iitk.ac.in
Manuscript received on 07 Feb 2002; Paper reviewed, revised and accepted on 08 Nov 2002

Paper presented at the 4th Annual CFD Symposium of the Aeronautical Society of India held on 10-11 August 2001 at Bangalore, India

Navier-Stokes equations governing incompressible fluid flow are

$$\rho\left(\frac{\partial \boldsymbol{u}}{\partial t}+\boldsymbol{u}.\nabla \boldsymbol{u}-\boldsymbol{f}\right)-\nabla.\boldsymbol{\sigma}= \quad \text{on } \Omega \quad \text{for } (0,T) \tag{1}$$

$$\nabla.\boldsymbol{u}=0 \quad \text{on } \Omega \quad \text{for } (0,T) \tag{2}$$

Hence $\rho, \boldsymbol{u}, \boldsymbol{f}$ and $\boldsymbol{\sigma}$ are the density, velocity, body force and the stress tensor respectively. The stress tensor is written as the sum of its isotropic and deviatoric parts

$$\boldsymbol{\sigma}=-p\boldsymbol{I}+\boldsymbol{T}, \boldsymbol{T}=2\mu\varepsilon(\boldsymbol{u}), \varepsilon(\boldsymbol{u})=1/2\left((\nabla \boldsymbol{u})+(\nabla \boldsymbol{u})^{T}\right), \tag{3}$$

where p and μ are the pressure and coefficient of dynamic viscosity respectively. Both the Dirichlet and Neumann type boundary conditions are accounted for, represented as

$$\boldsymbol{u}=\boldsymbol{g} \quad \text{on } \Gamma_g, \boldsymbol{n}.\boldsymbol{\sigma}=\boldsymbol{h} \quad \text{on } \Gamma_h, \tag{4}$$

where Γ_g and Γ_h are complimentary subsets of the boundary. The initial condition on the velocity is specified on Ω.

$$\boldsymbol{u}(\boldsymbol{x},0) = \boldsymbol{u}_0 \quad \text{on } \Omega \tag{5}$$

where $\mathbf{u}_0$ is divergence free.

Finite Element Formulation

Consider a finite element discretization of Ω into sub-domain Ω^e, e = 1,2,3, ..., n_{el}, where n_{el} is the number of elements. Based on this discretization, for velocity and pressure, we define the finite element trial function spaces S_u^h and S_p^h, and weighting function spaces V_u^h and V_p^h. The stabilized finite element formulation of equations (1) and (2) is written as follows : find $\boldsymbol{u}^h \in S_u^h$ and $p^h \in S_p^h$ such that $\forall\, \boldsymbol{w}^h \in V_u^h, q^h \in V_p^h$

$$\int_\Omega \boldsymbol{w}^h.\rho\left(\frac{\partial \boldsymbol{u}^h}{\partial t}+\boldsymbol{u}^h.\nabla \boldsymbol{u}^h-\boldsymbol{f}\right)d\Omega+\int_\Omega \boldsymbol{\varepsilon}(\boldsymbol{w}^h):\boldsymbol{\sigma}(p^h,\boldsymbol{u}^h)\,d\Omega$$

$$+\int_\Omega q^h\,\nabla.\boldsymbol{u}^h d\Omega+\sum_{e=1}^{n_{el}}\int_{\Omega^e}\frac{1}{\rho}\left(\tau_{SUPG}\,\rho\boldsymbol{u}^h.\nabla \boldsymbol{w}^h+\tau_{PSPG}\nabla q^h\right)\left[\rho\left(\frac{\partial \boldsymbol{u}^h}{\partial t}+\boldsymbol{u}^h.\nabla \boldsymbol{u}^h-\boldsymbol{f}\right)-\nabla.\boldsymbol{\sigma}(p^h,\boldsymbol{u}^h)\right]d\Omega^e$$

$$+\sum_{e=1}^{n_{el}}\int_{\Omega^e}\delta\nabla.\boldsymbol{w}^h\,\rho\nabla.\boldsymbol{u}^h\,d\Omega^e=\int_{\Gamma_h}\boldsymbol{w}^h.\boldsymbol{h}^h\,d\Gamma \tag{6}$$

In the variational formulation given by equation (6), the first three terms and the right hand side constitute the Galerkin formulation of the problem. The first series of the element level integrals are the SUPG and PSPG stabilization terms added to the variational formulation. In the current formulation τ_{PSPG} is the same as τ_{SUPG} and is given as

$$\tau=\left(2\,\|\boldsymbol{u}^h\|/h\right)^2+\left(4\nu/h^2\right)^2\Big)^{-1/2} \tag{7}$$

The second series of element level integrals are added to the formulation for numerical stability at high Reynolds numbers. This is a least squares terms based on the continuity equation. The coefficient δ is defined as

$$\delta = (h/2)\,\|\boldsymbol{u}^h\|\,z, \tag{8}$$

where,

$$z=\begin{cases}(Re_u/3), \mathrm{Re}_u \le 3\\ 1, \mathrm{Re}_u > 3\end{cases} \tag{9}$$

and Re_u is the cell Reynolds number. Both stabilization terms are weighted residuals, and therefore maintain the consistency of the formulation. h is the *element length* and various definitions have been used by researchers in the past. Mittal [7] conducted a systematic numerical study to investigate the effect of high aspect ratio elements on the performance of the finite element formulation for three commonly used definitions of h. The one which results in the least sensitivity of the computed flow to the element aspect ratio has been used for computations in the present work. According to this definition, the element is equal to the minimum edge length of a triangular (3 noded) element.

Power Spectra

The power spectrum is obtained by first calculating the two-dimensional discrete Fast Fourier Transform (FFT) of velocity field $\boldsymbol{u}(x,y,t)$. The Fourier coefficients $\hat{\boldsymbol{u}}(k_x, k_y, t)$ are defined as [8] :

$$\hat{\boldsymbol{u}}(k_x,k_y,t) = \frac{1}{\sqrt{N_x N_y}} \sum_{j_1=0}^{N_{x-1}} \sum_{j_2=0}^{N_{y-1}} \boldsymbol{u}(x,y,t) e^{-i((j_1 k_x/N_x)+(J_2 k_y/N_y))}, \quad (10)$$

while the inverse transform is defined as follows :

$$\boldsymbol{u}(x,y,t) = \sum_{k_x=0}^{N_{x-1}} \sum_{k_y=0}^{N_{y-1}} \hat{\boldsymbol{u}}(k_x, k_y, t) e^{-i((j_1 k_x/N_x)+(J_2 k_y/N_y))}, \quad (11)$$

Here, $k_x(n_1) = 2\pi n_1 / L_x$, $k_y(n_2) = 2\pi n_2 / L_y$, $n_i(n_2) = 0, \pm 1, \pm 2, \pm 3, \ldots$ and L_x and L_y are the length of the domain along x and y axes, respectively.

FFT is calculated using NAG library. The energy density, $\bar{E}$(k), corresponding to each discrete wavenumber is $\frac{1}{2}|\hat{\boldsymbol{u}}(k,t)|^2$, where $k = \sqrt{k_x^2 + k_y^2}$ .The energy $E(k)$ is calculated by integrating $E(k)$ over a thin shell of thickness $2\Delta k$. For discrete wavenumbers, $E(k)$ is computed by dividing the wavenumber space (in 2D) in a finite number of bands. Energy from FFT computations, whose corresponding wavenumber falls into a certain wavenumber band, is added up. The procedure can also be described as $E(k) = \sum_{k-\Delta k \le k \le k+\Delta k} \bar{E}(k_x, k_y)$.

The two invariant quantities in 2D isotropic turbulence are energy $(\int_\Omega E(k)\,dk)$ and enstrophy $(\int_\Omega |\omega|^2 d\Omega)$. Suppose energy is injected at a length scale $1/k_i$. The energy $E(k)$ varies as $E(k) \propto k^{-5/3}$ for $k \le k_i$ (due to energy invariance) and $E(k) \propto k^{-3}$ for $k > k_i$ (due to enstrophy invariance) [9, 10, 11].

The solution to Navier-Stokes equations is obtained for a non-uniform mesh. This solution is interpolated on a uniform mesh. In the present work, the effect of domain size and resolution of the uniform mesh on power spectra are studied. The effect of number of bands for k is also studied.

Results and Discussions

Equal-in-order linear basis functions for velocity and pressure are used and a 3-point Gaussian quadrature is employed for numerical integration. The non-linear equation systems resulting from the finite element discretization of the flow equations are solved using the Generalized Minimal RESidual (GMRES) technique [12] in conjunction with diagonal preconditioners. The finite element mesh consists of structured as well as unstructured grids of triangular elements. A structured grid that is extremely fine is employed close to the cylinder surface. It allows for good control over the distribution of elements in the boundary layer region. Farther away, an unstructured mesh is generated via Delaunay's triangulation. It is useful in saving computational costs. A picture of the mesh and its close up is shown in Fig.1.

The General Features of Flow

Computations are carried out for Re = 10^5, $2\text{x}10^5$, $4\text{x}10^5$, $6\text{x}10^5$, $8\text{x}10^5$ and 10^6. Fig.2 shows the time aver-

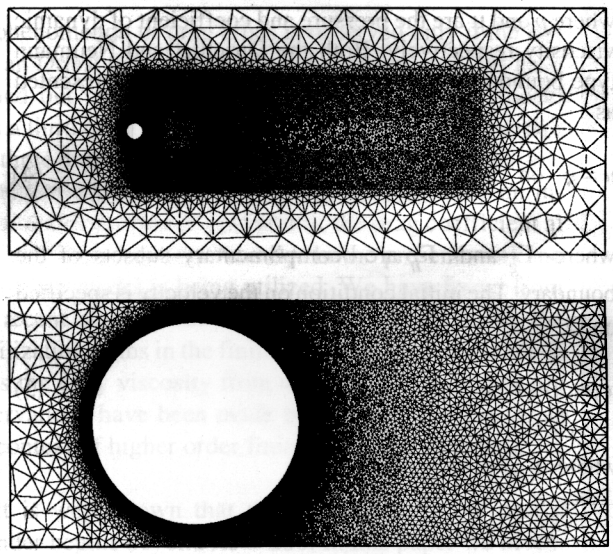

Fig. 1 Flow past a circular cylinder: typical finite element mesh with 47,011 nodes and 93,574 elements and its close up

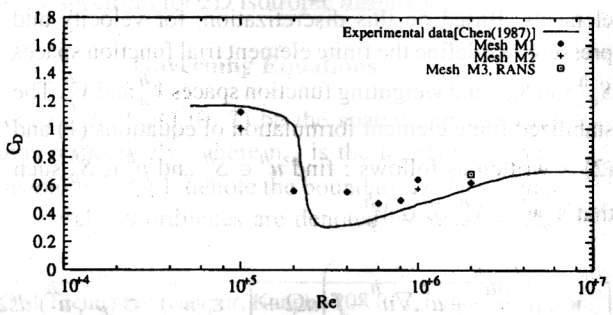

Fig. 2 Flow past a circular cylinder: mean drag coefficient for various Re. Mesh M1 consists of 47,011 nodes and 93,574 elements. Mesh M2 consists of 116,166 nodes and 231,484 elements. Mesh M3 has 22,403 nodes and 44,454 elements. The RANS computations utilises Balwin Lomax model for turbulence closure

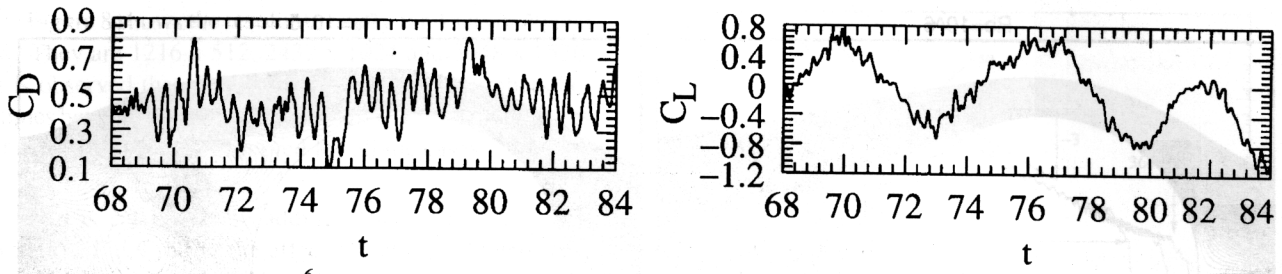

Fig. 3 Re=10^6 flow past a circular cylinder: time-histories of the drag (left) lift (right) coefficients

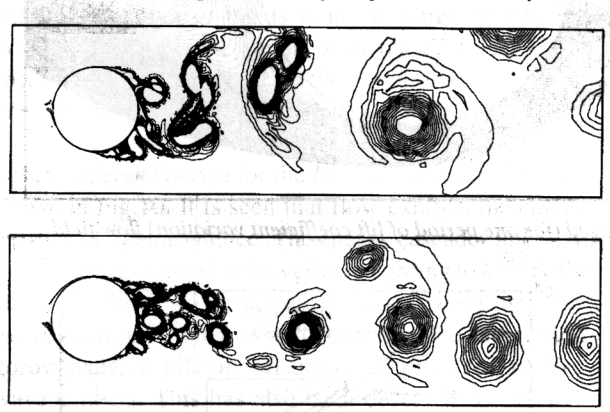

Fig. 4a Flow past a circular cylinder: instantaneous vorticity field (Re=10^5, top and Re=10^6, bottom)

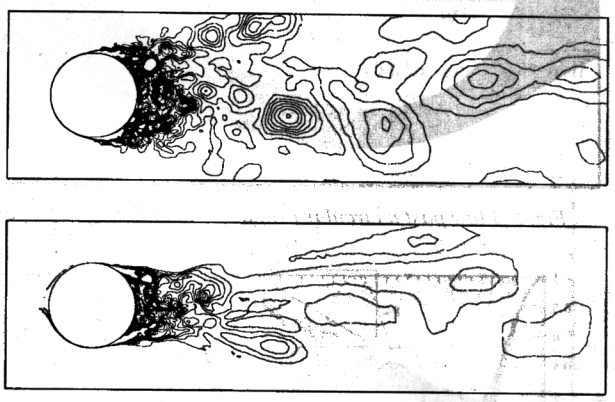

Fig. 4b Flow past a circular cylinder: time-averaged vorticity field (Re=10^5, top and Re=10^6, bottom)

aged drag-coefficient from the present computations for various Reynolds numbers. The experimental results, reported in Chen [13], are also shown in the figure. It can be seen that the phenomenon of drag crisis has been captured quite well. The drag coefficient drops suddenly at, approximately, $Re = 2\text{x}10^5$. The Reynolds number at which the phenomenon occurs matches quite well with the observations from experiments. The flow at low Re (< 1000) is associated with fairly regular vortex shedding. At high Reynolds numbers the vortices and their interactions are much stronger and the vortex shedding is not very regular. Consequently, the time averaging is a bit sensitive to the number of vortex shedding cycles for which the data is averaged if the number of vortex shedding cycles is not significantly large. This is why the C_D v/s Re variation is not very smooth. In the present work, because of the limitation of computational resources, the averaging has been done for about 5 vortex-shedding cycles. It is expected that the results will improve for a longer time-integration. Fig.3 shows the time-histories, for three vortex shedding cycles, approximately, of the drag (left) and lift (right) coefficients for the $Re = 10^6$ flow.

Instantaneous vorticity fields for $Re = 10^5$ and $Re = 10^6$ are shown in Fig.4(a). It is observed from the figure that the wake at $Re = 10^6$ is significantly narrower than that at $Re = 10^5$. The time-averaged (averaged over one cycle of lift coefficient) vorticity field is shown in Fig.4(b). The approximate locations of the separation point, with respect to the front stagnation point, are at angles 98 deg and 88 deg, for $Re = 10^6$ and $Re = 10^5$ respectively. The delay in the separation is even more apparent from the plot for the streamlines of the time-averaged flow shown in Fig.5. For the $Re = 10^5$ flow, a long bubble is observed close to the cylinder surface, immediately downstream of the point of separation. It is not observed for the flow at $Re = 10^6$. Possibly, at an intermediate Re, the laminar bubble bursts causing the flow separation to be delayed and resulting in a lower value of drag coefficient. The narrowing of the wake with the Reynolds number can also be observed from this figure.

Figure 6 shows the time-averaged pressure distribution on the surface of the cylinder. The drag coefficient for the potential flow is zero. In a real flow, because of the separation of flow, the pressure at the rear of the cylinder is lower than that in potential flow. The higher the base pressure, lower is the drag acting on the cylinder. One observes that the base pressure is higher for the flow at $Re = 10^6$ compared to that at $Re = 10^5$. Also shown in Fig.6 are the measurements from experiments [14]. Since the present computations are two-dimensional, as expected,

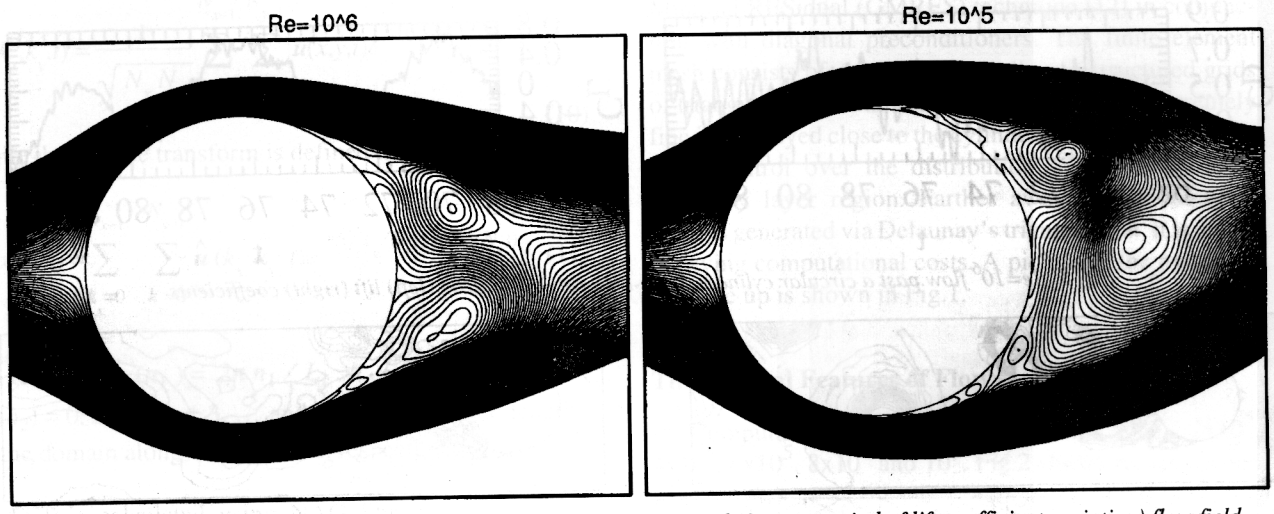

Fig. 5 Flow past a circular cylinder: streamlines for the time-averaged (for one period of lift coefficient variation) flow field

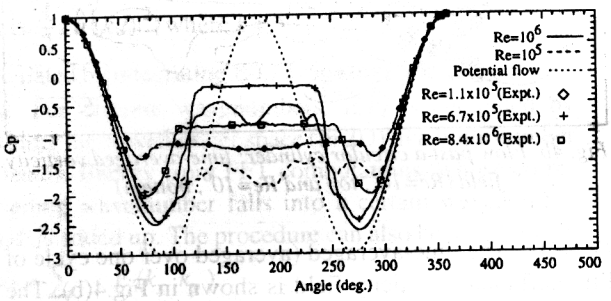

Fig. 6 Flow past a circular cylinder: pressure distribution on the surface of the cylinder for the time-averaged (for one period of lift coefficient variation) flow field

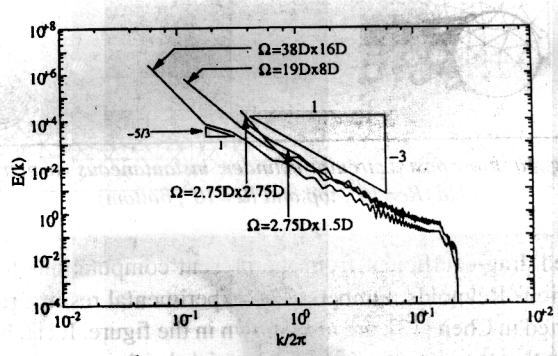

Fig. 7 Re=10^6 flow past a circular cylinder: energy spectra for different size of domain

there is some difference between the computational and experimental data. Qualitatively, the two sets of results match quite well. The increase in base pressure and delay of separation for the supercritical flow has been captured well by the present computations. This is very encouraging and more computations at intermediate *Re* will be carried out in future.

Energy Spectra

Four different domain sizes are considered to study the effect of domain size on power spectra. The details of these cases are presented in Table-1. Y_f is the extent of the upper and lower boundaries of the domain used for the FFT analysis from the cylinder center. X_{fu} is the location of the upstream edge of the domain from the cylinder. N_x and N_y are the number of nodes along the x and y axes, respectively for the mesh utilized for FFT. D is the diameter of the cylinder.

Table-1 : FFT of flow past a circular cylinder : values of parameters for various domains

Domain size	Y_f	X_{fu}	N_x x N_y
38D x 16D	8D	8D	2432 x 1024
19D x 8D	4D	4D	1216 x 512
2.75D x 2.75D	1.375D	1D	176 x 176
2.75D x 1.5D	0.75D	1D	176 x 96

The number of grid points along the x and y axes are taken such that resolution is same for all the cases. Energy spectra for all the domains are shown in Fig.7. We observe the presence of the -3 slope in all the cases and that of -5/3 only in the domain 38D x16D. The domain 38Dx16D is selected for further study since both the slopes are present in this case.

Figure 8 shows the resolution study for 3 sets of N_x and N_y. They are 1216 x 512, 2432 x 1024 and 3648 x 1536. It is observed that resolution of layer wave numbers becomes better as N_x and N_y are increased. Presence of slopes of -3 and -5/3 is also observed for all the cases.

$E(k)$ is calculated by adding $\overline{E}$ (k) over a thin shell around k. Fig.9 shows the effect of number of bands of k on energy spectra. Smooth variation of $E(k)$ is observed when the number of bands is in the range of 200-300. When the number of bands is increased to 2000, the spectrum becomes oscillatory. We see that both slopes are present when the number of band is around 300.

The energy spectra for the $Re = 10^5$ and 10^6 flows are shown in Fig.10. It is seen that flow exhibits the characteristics of 2D turbulence. The energy cascades at k^{-3}. An inverse energy cascade that varies according to $k^{-5/3}$ is also observed. Since no turbulence model is being used, and the resolution is not fine enough to resolve the Kolmogorov scale, a pile-up of energy is observed at large wavenumbers. This has also been observed by other researchers in the past [15]. This suggests that the numerical dissipation introduced by the stabilization terms is not enough to drain out the energy at large wavenumbers and an appropriate turbulence model is needed.

Conclusions

Computations have been carried out for flow past a circular cylinder at high Reynolds numbers. The phenomenon of drag crisis has been successfully simulated. The drop in drag is perhaps caused by the bursting of a laminar bubble close to the cylinder surface. This causes a delay in the separation of the flow and narrowing of the wake. The energy spectrum exhibits characteristics of 2D isotropic turbulence.

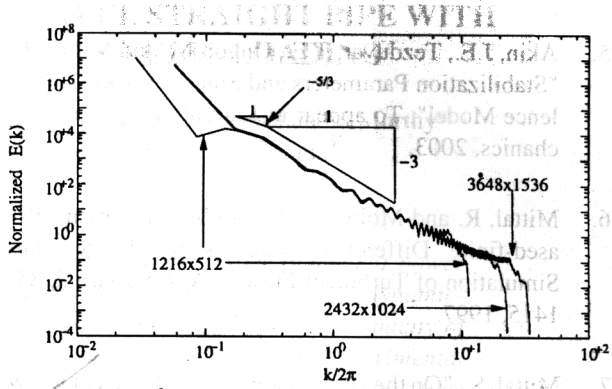

Fig. 8 Re=10^6 flow past a circular cylinder: energy spectra for various resolutions of the grid used for FFT

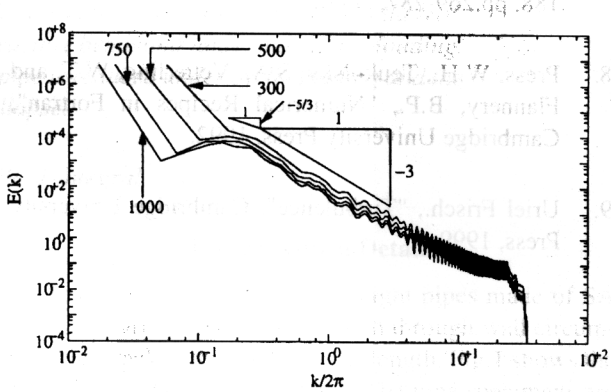

Fig. 9 Re=10^6 flow past a circular cylinder: energy spectra for various number of wave number bands

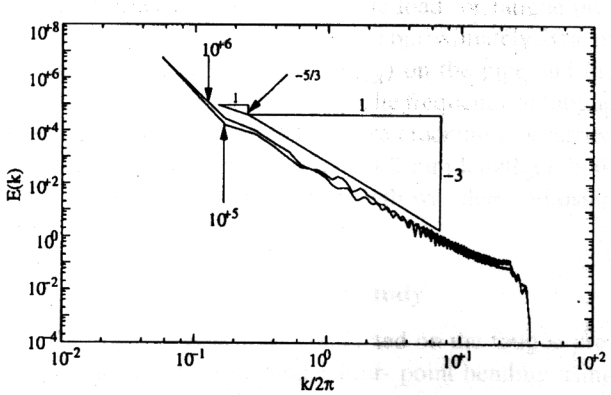

Fig. 10 Flow past a circular cylinder: comparison of the energy spectra for the Re=10^5 and 10^6 flows

References

1. White, F.M., Fluid Mechanics, McGraw Hill, 1994.

2. Williamson, C.H.K., "Vortex Dynamics in the Cylinder Wake", Annual Review Fluid Mechanics, 28, pp.477-539, 1996.

3. Selvam, R.P., "Finite Element Modeling of Flow Around a Circular Cylinder Using LES", Journal of Wind Engineering and Industrial Aerodynamics, 67 and 68, pp.129-139, 1997.

4. Tamura, T., Ohta, I. And Kuwahara, K., "On the Reliability of Two-Dimensional Simulation for Unsteady Flows Around a Cylinder-type Structure", Journal of Wind Engineering and Industrial Aerodynamics, 35, pp.275-298, 1990.

5. Akin, J.E., Tezduyar, T.E., Ungor, M. and Mittal, S., "Stabilization Parameters and Smaogorinsky Turbulence Model", To appear in Journal of Applied Mechanics, 2003.

6. Mittal, R. and Moin, P., "Suitability of Upwind-Biased-finite Difference Schemes for Large-Eddy Simulation of Turbulent Flows", AIAA Journal, 35, 1415, 1997.

7. Mittal, S., "On the Performance of High Aspect Ratio Elements for Incompressible Flows", Computer Methods in Applied Mechanics and Engineering, 188, pp.269-287, 2000.

8. Press, W.H., Teukolsky, S.A., Vetterling, W.T. and Flannery, B.P., "Numerical Recipes in Fortran", Cambridge University Press, 1992.

9. Uriel Frisch., "Turbulence", Cambridge University Press, 1999.

10. Paret, J. and Tabeling, P., "Intermittency in the Two-dimensional Inverse Cascade of Energy : Experimental Observations", Physics of Fluids, 10, pp.3126-3136, 1998.

11. Doering, C.R. and Gibbon, J.D., "Applied Analysis of the Navier-Stokes Equations", Cambridge University Press, 1995.

12. Saad, Y. and Schultz GMRES, M., "A Generalized Minimal Residual Algorithm for Solving Non-symmetric Linear Systems", SIAM Journal of Scientific and Statistical Computing, 7, pp.856-869, 1996.

13. Chen, S.S., "Flow Induced Vibration of Circular Cylindrical Structures", Springer Verlag, 1987.

14. Roshko, A., "Experiments on the Flow Past a Circular Cylinder at Very High Reynolds Number", Journal of Fluid Mechanics, 10, pp.345-356, 1961.

15. Mathieu, J. and Scott, J., "An Introduction to Turbulent Flow", Cambridge University Press, 2000.